Chalcogenide Letters Vol. 22, No. 9, September 2025, p. 787 - 796

Chemically deposited cubic SnS photocathodes for photoelectrochemical water splitting

U. Chalapathi [a], M. Vasudeva Reddy [b,c], C. P. Reddy [d], R. Dhanalakshmi [e], A. Divya [f], K. Mohanarangam [g], S. H. Park [a,*]

[a] *Department of Electronic Engineering, Yeungnam University, 280 Daehak-Ro, Gyeongsan, Gyeongbuk 38541, South Korea*

[b] *Department of Mathematics, Saveetha School of Engineering, Saveetha Institute of Medical and Technical Sciences (SIMATS), Thandalam, Chennai 602 105, India*

[c] *School of Chemical Engineering, Yeungnam University, Gyeongsan-si 38541, South Korea*

[d] *School of Science and Humanities, Department of Physics, Vel Tech Rangarajan Dr. Sagunthala R&D Institute of Science and Technology, Avadi, Chennai, India*

[e] *Department of Physics, University of Santiago of Chile (USACH), Santiago, Chile*

[f] *Department of Physics, School of Technology, The Apollo University, Chittoor, A.P., 517127, India*

[g] *Symbiosis Institute of Technology, Pune Campus, Symbiosis International (Deemed University), Pune, India*

Recently, cubic SnS shows promising potential for optoelectronic applications, including solar cells. Despite its advantages, the photoelectrochemical (PEC) properties of cubic SnS photoelectrodes remain underexplored. This study examines the PEC performance of cubic SnS photocathodes synthesized on FTO substrates via chemical bath deposition and annealed at 250°C for varying durations (10, 20, and 30 min). The as-deposited SnS films, characterized by a cubic crystal structure (lattice parameter: 1.162 nm, crystallite size: 17 nm), an energy gap of 1.75 eV, and an initial photocurrent of 0.8 mA/cm^2 at -1 V vs. Hg/HgO, showed significant enhancement upon annealing. A 10-minute annealing improved grain size and boosted the photocurrent to 1.4 mA/cm^2, while 20 minutes yielded optimized grain growth and uniformity, achieving 1.9 mA/cm^2. However, prolonged annealing (30 min) induced a secondary SnS_2 phase, reducing performance. These findings highlight the importance of controlled annealing for optimizing cubic SnS PEC performance.

(Received May 8, 2025; Accepted September 12, 2025)

Keywords: Cubic tin sulfide, Photocathodes, Chemical bath deposition, Energy gap, Photoelectrochemical cell

1. Introduction

In the current landscape of depleting fossil fuel reserves and escalating environmental degradation, there is an intensified research focus on alternative energy sources that are both clean and eco-friendly. Solar energy stands out as a prime candidate, offering an abundant and renewable resource that continuously bathes the Earth. Harnessing solar energy involves converting it into usable forms through photovoltaic (PV) and photoelectrochemical (PEC) processes. While PV cells utilize the photovoltaic effect to convert solar energy into electrical power, PEC cells generate hydrogen energy through water splitting. Hydrogen, with its high efficiency, light weight, and cleanliness, shows promise as a versatile energy carrier. Water splitting is a viable method for generating hydrogen energy, leveraging the ample amount of solar radiation. For efficient water splitting, the photoelectrode material should have optimal bandgap (1.0–2.0 eV) and electronic

* Corresponding author: sihyun_park@yu.ac.kr
https://doi.org/10.15251/CL.2025.229.787

properties, along with chemical stability, high catalytic activity, and scalability. Recently, n-type semiconductor photoelectrodes have gained significant attention for water splitting applications [1–5]. However, relatively little exploration has been conducted on p-type photoelectrodes, such as tin sulfide (SnS), despite its abundance and non-toxic nature. SnS crystallizes in orthorhombic, zinc blende, and cubic structures, based on the preparation conditions. While orthorhombic SnS is considered stable, the zinc blende and cubic phases are metastable [6–9]. Various groups have investigated the PV and PEC performance of orthorhombic SnS using a range of fabrication methods, yielding promising results [10–14]. The stable orthorhombic phase has demonstrated notable PEC and PV performance, with efficiencies of up to 4.2% in solar cells and photocurrent densities of 19 mA/cm^2 in PEC cells [10, 12]. In contrast, the cubic phase, characterized by a direct bandgap (~1.7 eV), high optical absorption, and excellent hole mobility (75 cm^2/V·s) [15], remains underexplored, particularly for PEC applications.

The synthesis of cubic tin sulfide (SnS) predominantly employs the chemical bath deposition (CBD) method, a straightforward, cost-effective, and scalable technique [16–23]. However, the formation of high-quality cubic SnS films is highly sensitive to bath temperature, precursor concentrations, solution pH, film thickness, annealing temperature, and doping levels. For instance, Garcia-Angelmo et al. [16] demonstrated that increasing the bath temperature from 20ºC to 40ºC transforms cubic SnS into its orthorhombic counterpart. Similarly, Javed et al. [20, 22] reported that doping with Fe reduced the bandgap from 1.74 eV to 1.63 eV, while increased film thickness shifted the bandgap from 1.70 eV to 1.74 eV. Marquez et al. [23] showed that raising the solution pH from 8.24 to 10.93 caused a phase transition from cubic to orthorhombic SnS. Further studies have explored the effects of various factors — such as ethylenediaminetetraacetic acid (EDTA) as a complexing agent, $Na_2S_2O_3$ concentration, annealing conditions, and dopants like Pb on the physical properties of cubic SnS [15, 24–28]. Annealing above 250ºC often induces SnS_2 formation, with complete conversion to SnS_2 at temperatures exceeding 350ºC. Kosuke et al. [9] and Kishore et al. [29] observed that reducing substrate or annealing temperatures to 250ºC preserved the cubic phase, while higher temperatures led to its degradation.

Maintaining the pure cubic phase of SnS is critical, as secondary phases like Sn_2S_3 and SnS_2 exhibit n-type conductivity and create deep traps, hindering carrier transport and degrading device performance. Therefore, precise optimization of deposition and annealing conditions is imperative to enhance phase purity and performance. In this study, cubic SnS films were deposited onto the FTO substrates using CBD under optimized conditions [27]. The films were annealed at 250ºC for 10, 20, and 30 minutes to refine crystallinity and phase purity. Shorter annealing durations (10–20 minutes) improved grain growth and homogeneity, with the 20-minute annealed film achieving a photocurrent of 1.9 mA/cm^2 at -1 V vs. Hg/HgO in a photoelectrochemical (PEC) cell. Conversely, prolonged annealing (30 minutes) resulted in SnS_2 secondary phases, underscoring the importance of controlled annealing for optimal PEC performance.

2. Experimental methods

Cubic SnS films were grown onto FTO substrates (sheet resistance: 15 Ω/□) using the CBD method. The chemical bath solution was prepared by dissolving 2.25 g of $SnCl_2 \cdot 2H_2O$ in 5 mL of acetone, followed by the sequential addition of 20 mL of 0.5 M EDTA (as a complexing agent), 12.5 mL of 1 M $Na_2S_2O_3$ (sulfur source), 12.5 mL of NH_4OH (pH adjuster), and 50 mL of deionized water. The deposition was conducted at 45ºC for 4 hours in a single cycle, yielding a thickness of approximately 1000 nm. Additional details on the deposition procedure are available in a previous study [27]. Post-deposition annealing was performed on the FTO/SnS photoelectrodes at 250ºC for 10, 20, and 30 minutes in a sulfur-rich atmosphere to enhance the crystallinity and phase purity of the cubic SnS films. The annealing conditions were carefully optimized to prevent the formation of secondary phases, with the film thickness remaining constant at 1000 nm after annealing for different durations. The physical and PEC properties of the prepared photoelectrodes were studied using X-ray diffraction (XRD), field-emission scanning electron microscopy (FESEM), energy-dispersive X-ray spectroscopy (EDS), UV-Vis-NIR spectroscopy, Hall measurements, and Corrtest electrochemical workstation [25,26].

3. Results and discussion

3.1. Structural analysis

The XRD profiles of the prepared and annealed FTO/SnS films at 250°C for 10, 20, and 30 minutes are presented in Figure 1. The as-grown film exhibits diffraction peaks characteristic of cubic SnS, consistent with reported literature [8, 30]. Peaks attributed to the underlying FTO substrate are also observed, marked with asterisks (*). The (222) and (400) planes dominate the diffraction pattern of the SnS films, while lower-intensity peaks correspond to the (211), (300), (410), (411), (421), (510), (440), (540), (622), and (444) planes, confirming the cubic phase of SnS. For the as-deposited films, the lattice parameter and crystallite size were estimated as 1.162 nm and 17 nm, respectively. Upon annealing at 250°C, a shift in the position of (222) peak from 26.55° to 26.65° was observed. This shift is attributed to strain induced in films during annealing. Additionally, after annealing for 30 minutes, a new diffraction peak emerged at 16.41°, corresponding to the (001) plane of SnS_2, as per JCPDS Card No. 023-0677. This peak indicates the onset of secondary phase formation due to prolonged annealing. The FWHM of the diffraction peaks remained relatively unchanged with annealing, suggesting that the crystallite size remained stable. However, the lattice parameter (a) exhibited a gradual decrease from 1.161 nm to 1.158 nm as the annealing duration increased from 10 to 30 minutes, which may be attributed to lattice strain and improved crystallinity. This study highlights the importance of annealing duration in obtaining the phase purity of SnS films. Short annealing durations (10–20 minutes) effectively maintain the cubic SnS phase, while extended annealing (30 minutes) formed SnS_2 secondary phases. The emergence of SnS_2 is undesirable for device applications due to its detrimental influence on the optoelectronic characteristics of the films. Therefore, precise optimization of annealing conditions is essential to ensure the fabrication of high-quality cubic SnS films suitable for practical use.

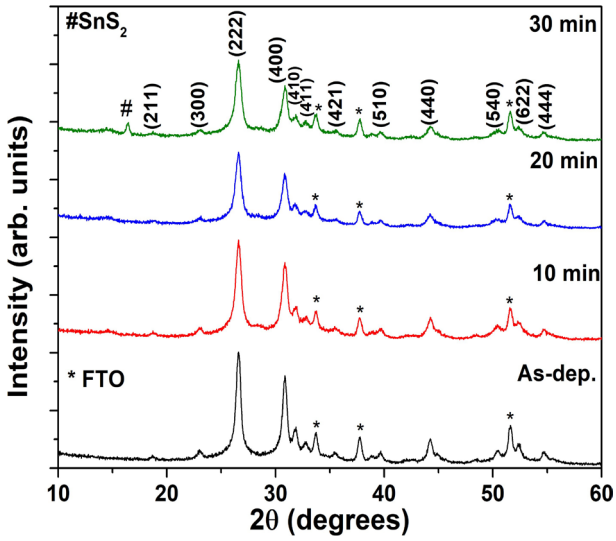

Fig. 1. XRD patterns of the prepared and annealed SnS films at 250°C for 10, 20, and 30 min.

3.2. Elemental analysis

The composition of films prepared on soda-lime glass substrates was analyzed using EDS. Table 1 summarizes the composition data for both the as-prepared and those annealed at 250°C for 10, 20, and 30 minutes. The as-deposited films exhibited a non- stoichiometric composition, characterized by being Sn-rich and S-deficient, with a sulfur-to- tin (S/Sn) ratio of 0.80. Upon annealing at 250°C, a progressive increase in the sulfur atomic percentage was observed, accompanied by a corresponding decrease in the tin atomic percentage as the annealing duration increased. Specifically, the S/Sn ratio improved steadily, reaching 0.94 for films annealed in 30

minutes. This compositional adjustment indicates that annealing in a sulfur atmosphere facilitates the inclusion of sulfur into the SnS films, thereby moving the composition closer to stoichiometry. The nearly stoichiometric composition achieved after 30 minutes of annealing underscores the importance of annealing duration and conditions in optimizing the elemental balance of SnS films, which is critical for their structural and functional properties.

Table 1. Composition data of the prepared and annealed SnS films at 250°C for 10, 20, and 30 min.

Sample	Sn (at.%)	S (at.%)	S/Sn ratio
As-dep.	55.5	44.5	0.80
10 min	54.3	45.7	0.84
20 min	53.4	46.6	0.87
30 min	51.5	48.5	0.94

3.3. Morphology

Figure 2 displays the surface morphologies cross-sections of the prepared films. The as-deposited film features micron-sized grains composed of agglomerated nanoparticles uniformly distributed over the substrate. After annealing at 250°C for 10 min, the distinct nanoparticle features begin to merge into the grains due to the coalescence phenomenon induced by heating. Extending the annealing time from 10 to 20 min improves the grain size, compactness, and uniformity. The cross-section of the 20 min annealed film reveals the vertical growth of a compact and uniform layer with a thickness of 1000 nm on the FTO layer (600 nm). The surface morphology is like those reported for cubic SnS films prepared via CBD method [16, 23]; however, the achieved film thickness and grain sizes are superior to those reported in previous works on cubic SnS [16–23]. Further annealing at 30 min results in more uniform grain growth, accompanied by fine white flakes on the grain surfaces corresponding to the SnS_2 secondary phase [25, 26]. This observation clearly indicates that annealing durations exceeding 20 min are not beneficial from a microstructure standpoint.

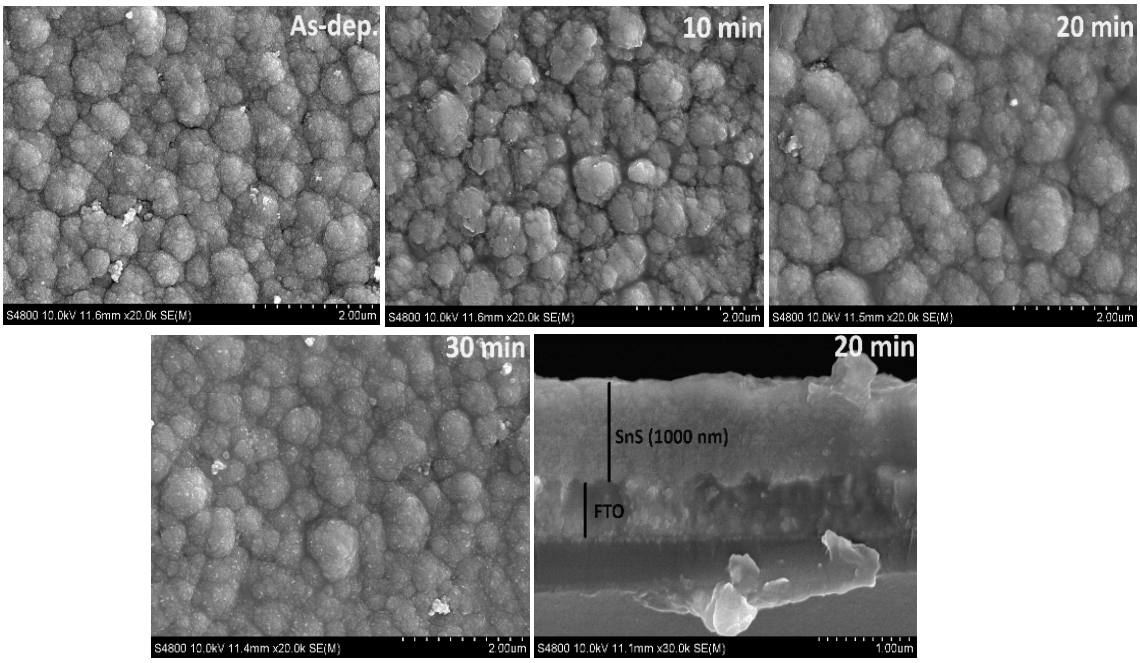

Fig. 2. FESEM images of the prepared and annealed SnS films at 250°C, and the cross-sectional image of the film annealed for a duration of 20 min.

3.4. Optical absorption

Figure 3 shows the transmittance and reflectance spectra of both the prepared and annealed films at 250°C for durations of 10 to 30 min. The as-deposited film exhibits 40% transmittance and 45% reflectance at longer wavelengths, with an absorption onset from 810 to 650 nm. This absorption onset aligns with previously reported data for cubic SnS [8, 16, 17]. Upon annealing at 250°C for 10 to 30 min, improvements in transmittance and reflectance are observed, attributed to the enhanced grain size evident in the micrographs.

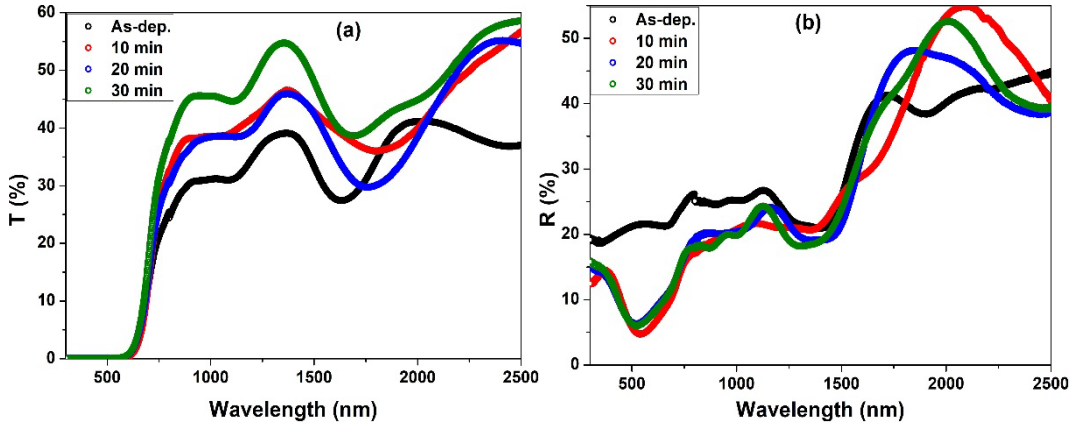

Fig. 3. (a) Transmittance and (b) reflectance curves of the prepared and annealed films at 250°C for 10, 20, and 30 min.

However, there is no significant shift in the absorption onset with increasing annealing duration, indicating that the bandgap of the films remains largely unchanged upon annealing at 250°C.

Figure 4 illustrates the $(\alpha h\nu)^2$ versus $h\nu$ plots, employed to estimate the optical bandgap of the SnS films. The optical bandgap of the as-prepared and those annealed for 10 minutes was calculated to be 1.75 eV. After 20 minutes of annealing, the bandgap showed a slight reduction to 1.74 eV, followed by an increase to 1.76 eV for films annealed for 30 minutes. These variations in the bandgap are attributed to the changes in crystallinity, stoichiometry, and the emergence of secondary phases during annealing. The observed bandgap values align well with the reported values of cubic SnS [8, 16, 17], confirming the successful synthesis of cubic SnS with high phase purity under optimized annealing conditions.

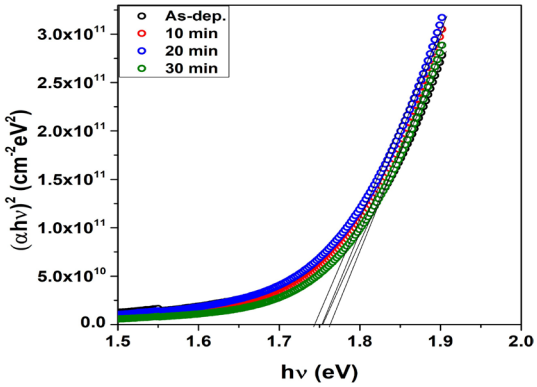

Fig. 4. $(\alpha h\nu)^2$ versus $h\nu$ curves of the prepared and annealed SnS films at 250°C for 10, 20, and 30 min.

3.5. Electrical properties

The electrical properties of the films are listed in Table 2. All films exhibited p-type conductivity. For the as-deposited films, the electrical resistivity, hole mobility, and carrier concentration were measured as 1.5×10^4 Ω.cm, 35.2 $cm^2V^{-1}s^{-1}$, and 8.2×10^{12} cm^{-3}, respectively. After annealing at 250°C for 10 minutes, the electrical resistivity increased to 4.1×10^4 Ω.cm, and the hole mobility significantly improved to 78 $cm^2V^{-1}s^{-1}$, while the carrier concentration decreased to 1.8×10^{12} cm^{-3}. Upon extending the annealing duration to 20 minutes, the resistivity, mobility, and carrier concentration further improved to 5.4×10^4 Ω.cm, 90 $cm^2V^{-1}s^{-1}$, and 2.0×10^{12} cm^{-3}, respectively. These improvements in resistivity and mobility, alongside the reduction in carrier concentration, are attributed to enhanced stoichiometry, grain size, and film homogeneity due to sulfur incorporation during annealing. However, with a 30-minute annealing duration, the resistivity and carrier concentration increased to 1.35×10^5 Ω.cm and 8.5×10^{12} cm^{-3}, respectively, while the hole mobility decreased to 25 $cm^2V^{-1}s^{-1}$. This decline in electrical performance is associated with the emergence of the undesirable SnS_2 secondary phase, which degrades the film's quality and electrical properties.

Table 2. Electrical properties of the prepared and annealed SnS films at 250°C for 10, 20, and 30 min.

Sample	Annealing duration	Resistivity (Ω.cm)	Mobility ($cm^2V^{-1}s^{-1}$)	Carrier concentration (cm^{-3})
As-dep.	–	$1.5x10^4$	35.2	$8.2x10^{12}$
Annealed	10 min	$4.1x10^4$	78.0	$1.8x10^{12}$
Annealed	20 min	$5.4x10^4$	90.0	$2.0x10^{12}$
Annealed	30 min	$1.3x10^5$	25.0	$8.5x10^{12}$

The measured electrical properties are consistent with the reported values of cubic SnS. For instance, Garcia et al. [16, 17] and Kishore et al. [29] reported resistivity values for cubic SnS films ranging from 101 to 107 Ω.cm, with variations in mobility and carrier concentration influenced by annealing conditions. Specifically, Kishore et al. observed resistivity values between 29.4 and 376.5 Ω.cm, mobility ranging from 13.1 to 66.1 $cm^2V^{-1}s^{-1}$, and carrier concentrations of 4.2×10^{14} to 3.0×10^{16} cm^{-3} as the annealing temperature increased from 350°C to 500°C in sprayed films. In this study, the films annealed for 20 minutes demonstrated optimal electrical properties, characterized by a favorable balance of resistivity, mobility, and carrier concentration. These results indicate that films annealed under these conditions are well-suited for water splitting.

3.6. Photoelectrochemical performance

The linear sweep voltammetry (LSV) curves of the prepared photoelectrodes are shown in Figure 5. The cathodic photoresponse observed in all samples confirms their p-type conductivity [31, 32]. Under illumination, distinct photoresponses are observed for both the as-prepared and annealed photocathodes. The as-prepared photocathode exhibits a photocurrent density of 0.8 mA/cm^2 at −1.0 V (vs. Hg/HgO). Annealing at 250°C for 10 minutes improves the photocurrent to 1.4 mA/cm^2, attributed to enhanced crystalline and stoichiometry of the films. A further increase in photocurrent to 1.9 mA/cm^2 is observed for films annealed at 250°C for 20 minutes. This improvement correlates with an increase in grain size, improved homogeneity, and reduced defect states in the films, as evidenced by the FESEM images. However, extending the annealing duration to 30 minutes results in a decline in photocurrent to 1.2 mA/cm^2. This decrease in photocurrent can be attributed to the evolution of SnS_2 phase. The SnS_2 phase introduces deep trap states, which hinder the transport of charge carriers, and reduces the PEC performance. These results revealed the importance of annealing duration in optimizing the PEC performance of cubic SnS photoelectrodes, with the 20-minute annealing condition yielding the best performance.

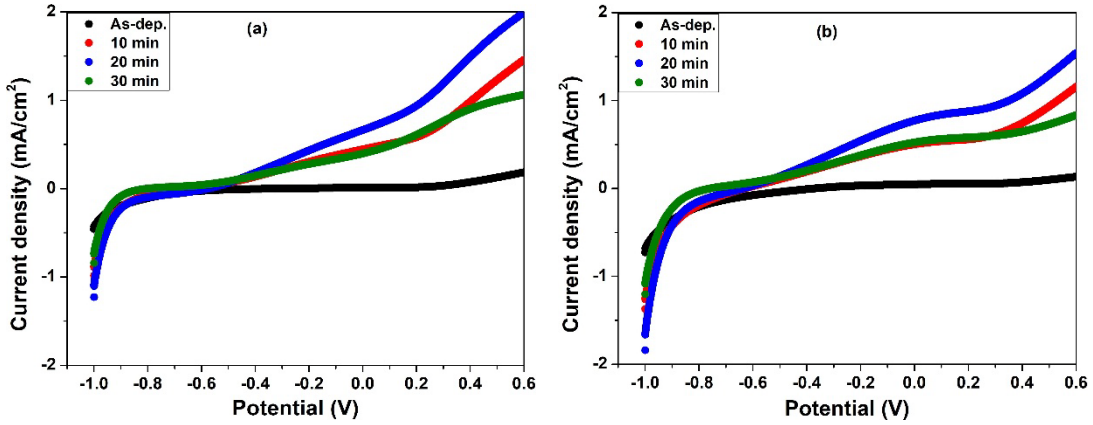

Fig. 5. LSV curves of the prepared and annealed SnS films at 250°C for 10, 20, and 30 min measured under (a) dark and (b) illumination.

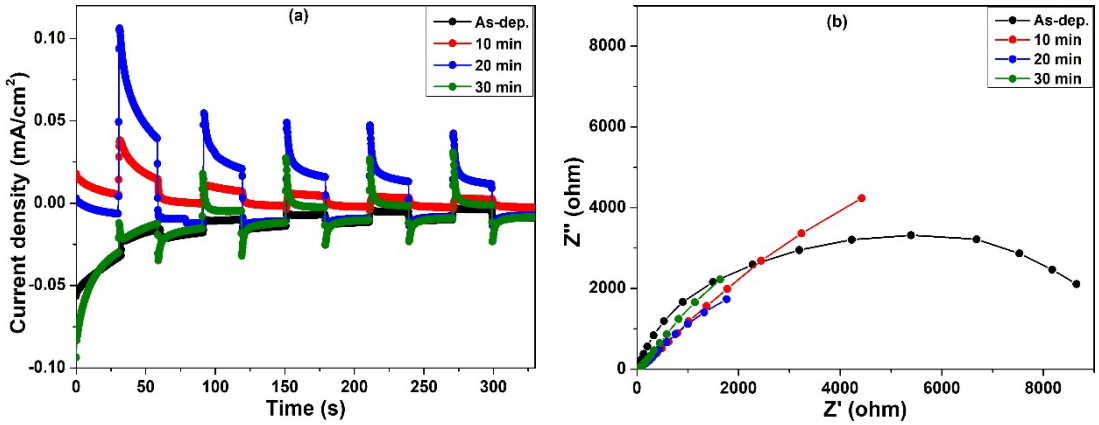

Fig. 6. (a) J-t and (b) Nyquist plots measured at -0.5 V for the as-prepared and annealed SnS films at 250°C for 10, 20, and 30 min.

The photocurrent vs. time (I-T) curves of the as-prepared and annealed photoelectrodes, recorded over a 330-second duration, are presented in Figure 6(a) to assess their stability under continuous illumination. The as-deposited photocathode exhibits a low and relatively stable photocurrent of -0.01 mA/cm^2 at a bias voltage of -0.5 V throughout the 330 s duration, suggesting poor charge separation and limited photocurrent generation. In contrast, the photocathode annealed at 250°C for 10 minutes shows an enhanced and sustained photocurrent of 0.03 mA/cm^2, indicating improved charge separation and better film quality. The photocurrent increases further to 0.1 mA/cm^2 with a 20-minute annealing duration, reflecting enhanced grain size, crystallinity, and overall stability of the photocathode. However, when the annealing time increases to 30 minutes, the photocurrent declines back to -0.01 mA/cm^2, likely due to the formation of the SnS_2 secondary phase, which introduces deep trap states and reduces the photocurrent. The improved photocurrent observed for the photocathodes annealed for 10 and 20 minutes suggests enhanced grain size, which facilitates better charge separation and improves the long-term stability of the photocathode.

Figure 6(b) presents the Nyquist plots, recorded at -0.5 V bias potential. The as-deposited photocathode exhibits prominent semi-circular behavior, indicative of charge transfer processes at the electrode-electrolyte interface. The larger semi-circle observed for the as-deposited photocathode suggests higher charge-transfer resistance [33, 34], likely caused by surface imperfections or contaminants introduced during the CBD process. After annealing at 250°C for 10, 20, and 30 minutes, the Nyquist plots transition from a full semi-circle to a half-semicircle, signaling a reduction in charge-transfer resistance and improved electrical properties. The decrease in charge-transfer resistance is attributed to enhanced crystallinity, better interface quality, and a reduction in

defects following the annealing process. The photocathode annealed for 20 minutes exhibits the smallest half-semicircle, indicating the lowest charge-transfer resistance, which is a result of improved grain growth and phase purity during the annealing process. This trend emphasizes the beneficial impact of controlled annealing on the electrical performance of SnS-based photocathodes.

4. Conclusions

In this study, cubic SnS photocathodes were successfully grown on FTO substrates using CBD and annealing at 250°C for durations ranging from 10 to 30 minutes. A comprehensive analysis of the physical and PEC properties of the prepared samples was conducted. Structural analysis confirmed the crystallization of cubic SnS with a lattice parameter of 1.162 nm, which slightly decreased from 1.161 nm to 1.158 nm as the annealing duration increased from 10 to 30 minutes. Notably, after 30 minutes of annealing, the emergence of the SnS_2 secondary phase was observed. Compositional analysis revealed that the as-prepared films were sulfur- deficient, but the sulfur content gradually improved, approaching near-stoichiometry with longer annealing times at 250°C. Morphological analysis showed significant improvements in grain size and uniformity for films annealed for 10 to 20 minutes, while SnS_2 nanoflakes began to form on the grain surfaces after 30 minutes of annealing. Optical absorption studies indicated increased transmittance with longer annealing durations, with direct bandgaps of 1.75 eV for the as-prepared, and 1.75, 1.74, and 1.76 eV for films annealed for 10, 20, and 30 minutes, respectively.

Hall measurements demonstrated a significant increase in hole mobility from 35.2 to 90 $cm^2V^{-1}s^{-1}$ as the annealing time increased from 10 to 20 minutes, followed by a decrease to 25 $cm^2V^{-1}s^{-1}$ after 30 minutes of annealing. PEC measurements showed a substantial enhancement in photocurrent from 0.8 to 1.9 mA/cm^2 after annealing the as-deposited films at 250°C for 10 to 20 minutes. However, the photocurrent decreases to 1.2 mA/cm^2 at a 30-minute annealing duration, likely due to the evolution of SnS_2 secondary phase. Remarkably, the SnS photocathode annealed for 20 minutes demonstrated stable photocurrent over 330 seconds under illumination, indicating its potential for long-term PEC water splitting applications. Overall, these findings confirm the suitability of the prepared cubic SnS photocathodes, particularly those annealed for 20 minutes, for efficient PEC water splitting. The results highlight the important role of annealing duration in optimizing SnS properties for renewable energy applications.

Acknowledgement

This research was supported by the Gyeongsangbuk-do RISE(Regional Innovation System & Education) project.

References

[1] Y. Kuang, Q. Jia, H. Nishiyama, T. Yamada, A. Kudo, K. Domen, Adv. Energy Mater. 6 (2016) 1501645; https://doi.org/10.1002/aenm.201501645

[2] C. Liu, Y. Yang, W. Li, J. Li, Y. Li, Q. Chen, Chem. Eng. J. 302 (2016) 717-724; https://doi.org/10.1016/j.cej.2016.05.126

[3] Z. Wu, D. Yuan, S. Lin, W. Guo, D. Zhan, L. Sun, C. Lin, Int. J. Hydrogen Energy 45 (2020) 32012-32021; https://doi.org/10.1016/j.ijhydene.2020.08.258

[4] B. Giri, M. Masroor, T. Yan, K. Kushnir, A. D. Carl, C. Doiron, H. Zhang, Y. Zhao, A. McClelland, G. A. Tompsett, D. Wang, R. L. Grimm, L. V.Titova, P. M. Rao, Adv. Energy Mater. 9 (2019) 1901236; https://doi.org/10.1002/aenm.201901236

[5] C. Zhu, C. Liu, Y. Zhou, Y. Fu, S. Guo, H. Li, S. Zhao, H. Huang, Y. Liu, Z. Kang, Appl. Catal. B: Environ. 216 (2017) 114-121; https://doi.org/10.1016/j.apcatb.2017.05.049

[6] Z. Deng, D. Han, Y. Liu, Nanoscale 3 (2011) 4346-4351; https://doi.org/10.1039/c1nr10815h

[7] A. Rabkin, S. Samuha, R. E. Abutbul, V. Ezersky, L. Meshi, Y. Golan, Nano Lett. 15 (2015) 2174-2179; https://doi.org/10.1021/acs.nanolett.5b00209

[8] R. Abutbul, E. Segev, L. Zeiri, V. Ezersky, G. Makov, Y. Golan, RSC Adv. 6 (2016) 5848-5855; https://doi.org/10.1039/C5RA23092F

[9] K. O. Hara, S. Suzuki, N. Usami, Thin Solid Films 639 (2017) 7-11; https://doi.org/10.1016/j.tsf.2017.08.025

[10] P. Sinsermsuksakul, J. Heo, W. Noh, A. S. Hock, R. G. Gordon, Adv. Energy Mater. 1 (2011) 1116-1125; https://doi.org/10.1002/aenm.201100330

[11] T.-T. Ho, E. Jokar, S. Quadir, R.-S. Chen, F.-C. Liu, C.-Y. Chen, K.-H. Chen, L.-C. Chen, Sol. Energy Mater. Sol. Cells 236 (2022) 111499; https://doi.org/10.1016/j.solmat.2021.111499

[12] H. Lee, W. Yang, J. Tan, J. Park, S. G. Shim, Y. S. Park, J. W. Yun, K. M. Kim, J. Moon, ACS Appl. Mater. Interf. 12 (2020) 15155-15166; https://doi.org/10.1021/acsami.9b23045

[13] W. Zhang, Y. Cheng, J. Zhao, Q. Li, J. Wang, J. Zhu, H. Miao, X. Hu, J. Phys. D: Appl. Phys. 55 (2022) 165502; https://doi.org/10.1088/1361-6463/ac472e

[14] A. Singh, J. Rohilla, M. S. Hassan, P. P. Ingole, P. K. Santra, D. Ghosh, S. Sapra, ACS Appl. Nano Mater. 5 (2022) 4293-4304; https://doi.org/10.1021/acsanm.2c00233

[15] U. Chalapathi, B. Poornaprakash, S.-H. Park, Sol. Energy 139 (2016) 238-248; https://doi.org/10.1016/j.solener.2016.09.046

[16] A. R. Garcia-Angelmo, M. Nair, P. Nair, Solid State Sci. 30 (2014) 26-35; https://doi.org/10.1016/j.solidstatesciences.2014.02.002

[17] A. Garcia-Angelmo, R. Romano-Trujillo, J. Campos-A'lvarez, O. Gomez-Daza, M. Nair, P. Nair, Phys. Status Solidi A 212 (2015) 2332-2340; https://doi.org/10.1002/pssa.201532405

[18] P. Nair, A. Garcia-Angelmo, M. Nair, Phys. Status Solidi A 213 (2016) 170-177; https://doi.org/10.1002/pssa.201532426

[19] M. S. Mahdi, K. Ibrahim, A. Hmood, N. M. Ahmed, F. I. Mustafa, S. A. Azzez, Mater. Lett. 200 (2017) 10-13; https://doi.org/10.1016/j.matlet.2017.04.077

[20] A. Javed, Q. ul Ain, M. Bashir, J. Alloy. Compd. 759 (2018) 14-21; https://doi.org/10.1016/j.jallcom.2018.05.158

[21] V. E. Gonz'alez-Flores, R. N. Mohan, R. Ballinas-Morales, M. Nair, P. Nair, Thin Solid Films 672 (2019) 62-65; https://doi.org/10.1016/j.tsf.2018.12.044

[22] A. Javed, N. Khan, S. Bashir, M. Ahmad, M. Bashir, Mater. Chem. Phys. 246 (2020) 122831; https://doi.org/10.1016/j.matchemphys.2020.122831

[23] I. Marquez, R. Romano-Trujillo, J. Gracia-Jimenez, R. Galeazzi, N. Silva-Gonz'alez, G. Garc'ıa, A. Coyopol, F. Nieto-Caballero, E. Rosendo, C. Morales, J. Mater. Sci.: Mater. Electron. 32 (2021) 15898-15906; https://doi.org/10.1007/s10854-021-06141-9

[24] U. Chalapathi, B. Poornaprakash, S.-H. Park, J. Alloy. Compd. 689 (2016) 938-944; https://doi.org/10.1016/j.jallcom.2016.08.066

[25] U. Chalapathi, B. Poornaprakash, S.-H. Park, Superlattice. Microst. 103 (2017) 221-229; https://doi.org/10.1016/j.spmi.2017.01.034

[26] U. Chalapathi, B. Poornaprakash, B. Purushotham Reddy, S.-H. Park, Thin Solid Films 640 (2017) 81-87; https://doi.org/10.1016/j.tsf.2017.09.004

[27] U. Chalapathi, B. Poornaprakash, W. J. Choi, S.-H. Park, Appl. Phys. A 126 (2020) 583; https://doi.org/10.1007/s00339-020-03763-4

[28] U. Chalapathi, Y. Jayasree, S.-H. Park, Mater. Sci. Semicon. Proc. 150 (2022) 106958; https://doi.org/10.1016/j.mssp.2022.106958

[29] T. Kishore Bhat, K. Jeganath, S. D. George, Y. Raviprakash, J. Mater. Sci.: Mater. Electron. 34 (2023) 747; https://doi.org/10.1007/s10854-023-10157-8

[30] R. Abutbul, A. Garcia-Angelmo, Z. Burshtein, M. Nair, P. Nair, Y. Golan, CrystEngComm 18 (2016) 5188-5194; https://doi.org/10.1039/C6CE00647G

[31] W. Gao, C. Wu, M. Cao, J. Huang, L. Wang, Y. Shen, J. Alloy. Compd. 688 (2016) 668-674; https://doi.org/10.1016/j.jallcom.2016.07.083

[32] J. Jing, M. Cao, C. Wu, J. Huang, J. Lai, Y. Sun, L. Wang, Y. Shen, J. Alloy. Compd. 726 (2017) 720-728; https://doi.org/10.1016/j.jallcom.2017.07.303

[33] Y. Wang, W. Tian, L. Chen, F. Cao, J. Guo, L. Li, ACS Appl. Mater. Inter. 9 (2017) 40235-40243; https://doi.org/10.1021/acsami.7b11510

[34] S. Sharma, D. Kumar, N. Khare, Int. J. Hydrogen Energy 44 (2019) 3538-3552; https://doi.org/10.1016/j.ijhydene.2018.11.238